Two-photon calcium imaging from head-fixed *Drosophila* during optomotor walking behavior

Johannes D Seelig[1,2], M Eugenia Chiappe[1,2], Gus K Lott[1,2], Anirban Dutta[1], Jason E Osborne[1], Michael B Reiser[1] & Vivek Jayaraman[1]

***Drosophila melanogaster* is a model organism rich in genetic tools to manipulate and identify neural circuits involved in specific behaviors. Here we present a technique for two-photon calcium imaging in the central brain of head-fixed *Drosophila* walking on an air-supported ball. The ball's motion is tracked at high resolution and can be treated as a proxy for the fly's own movements. We used the genetically encoded calcium sensor, GCaMP3.0, to record from important elements of the motion-processing pathway, the horizontal-system lobula plate tangential cells (LPTCs) in the fly optic lobe. We presented motion stimuli to the tethered fly and found that calcium transients in horizontal-system neurons correlated with robust optomotor behavior during walking. Our technique allows both behavior and physiology in identified neurons to be monitored in a genetic model organism with an extensive repertoire of walking behaviors.**

Drosophila melanogaster has a brain of only about 100,000 neurons but displays a wide variety of behaviors[1], ranging from innate behaviors like phototaxis and courtship, to adaptive behaviors such as remembering associations between sensory stimuli and conditional reward or punishment. Genetic tools to manipulate the activity of defined subpopulations of neurons in the fly brain have helped identify candidate neural substrates for many of these behaviors, but it has been harder to establish clear links between behavior and neural activity. Physiological recordings from the fly's brain can provide such a link, but these recordings are made challenging in the fly because of its small size. Technical advances in the past decade have improved the fly physiologist's tool kit, making it possible to use powerful circuit-busting strategies that combine physiology analyses with genetic and behavioral tools[2–4].

Studies of adult fly brain function now routinely use either genetically encoded sensors and/or electrophysiology experiments to record the activity of identified neural populations in a fixed fly. Electrophysiology data have high temporal resolution and, in the case of somatic whole-cell patch-clamp recordings, provide a window into synaptic activity that is difficult to obtain using other methods. But much of the processing in insect neurons is localized to arbors that are distant from the soma[5–7], and these arbors are difficult to target with patch-clamp recordings. Increasingly powerful imaging techniques thus provide a complementary capability to monitor neural activity. In *Drosophila*, two-photon imaging[8] with genetically encoded sensors is a relatively noninvasive means of recording neural activity from identified neurons at high spatial resolution[9–11].

However, recording in a completely immobilized preparation is not sufficient to directly connect neural activity and behavior. Recording neural activity while the fly is engaged in a task allows for a direct exploration of the functional properties of a circuit in the context of the behavior. Feedback from other brain areas is likely to be important in neural circuit operation during fly behavior. Such recordings enable investigations into the links between neural and behavioral variability during individual trials[12]. Recordings in head-fixed flies give a high degree of control over stimulus presentation and have been used in the past in insects[13–15], primates[16,17] and rodents[18,19].

We developed a head-fixed, behaving-fly preparation and demonstrated its use by recording from motion-sensitive lobula plate tangential cells (LPTCs) of the optic lobe during walking behavior. LPTCs have been the focus of many investigations in larger blowflies (*Calliphora* sp.)[20,21] and have recently been the target of physiological studies in *Drosophila* as well[15,22,23]. Here we used two-photon imaging with GCaMP3.0 (ref. 24) to record dendritic calcium responses of the horizontal system (HS) neurons of the lobula plate in *Drosophila*. In stationary flies, HS-neuron responses to optic flow were similar to those previously observed[23,25–27] (M.E.C., J.D.S., M.B.R. and V.J.; unpublished data). In walking flies, on average, optomotor responses to motion stimuli in the preferred direction of HS neurons followed and were correlated with neuronal responses, as has only been predicted previously[25]. Our technique thus enables measurements of neural activity in genetically targeted cell populations during behavior and under sensory stimulation that is relevant to the neurons under study.

[1]Janelia Farm Research Campus, Howard Hughes Medical Institute, Ashburn, Virginaia, USA. [2]These authors contributed equally to this work. Correspondence should be addressed to V.J. (vivek@janelia.hhmi.org).

RECEIVED 10 FEBRUARY; ACCEPTED 6 MAY; PUBLISHED ONLINE 6 JUNE 2010; CORRECTED AFTER PRINT 10 JANUARY 2011; DOI:10.1038/NMETH.1468

RESULTS

Experimental setup

The fly's small size poses the main challenge in performing physiology experiments under conditions that permit behavior. In most *in vivo Drosophila* physiology experiments, flies are fixed in positions that prevent natural movement of their legs and wings. Our modified holder allowed walking behavior under visual stimulation (**Supplementary Movie 1**). The holder also permitted physiology experiments with comfortable access to the brain for dissection and imaging under a water-immersion objective. A 0.001-inch-thick (0.0254 mm) stainless steel shim fly holder separates the dorsal side of the head, the neck and a part of the thorax from the rest of the fly. We cut an opening that accommodates parts of the fly's head and thorax into the shim using a laser mill (**Supplementary Figs. 1** and **2a**). Then we glued the fly holder with epoxy into a three-dimensional printer–constructed photopolymer resin chamber that forms the bottom of the liquid chamber, which provides a fluid volume for a water-immersion objective (**Fig. 1a**). We mounted the fly in the holder in a manner similar to that used in many tethered fly behavioral experiments[28] (**Supplementary Fig. 2b**). During dissection, we removed the cuticle and some of the fat tissue from the fly that prevented optical access to the LPTCs. We minimized brain movement by fixing the proboscis and removing muscles that are known to cause brain motion[10]. This was sufficient to largely eliminate central brain motion, but additional muscles near the optic lobes appear to move the lateral parts of the brain, often during visual stimulation[29], and these prevented complete brain stabilization.

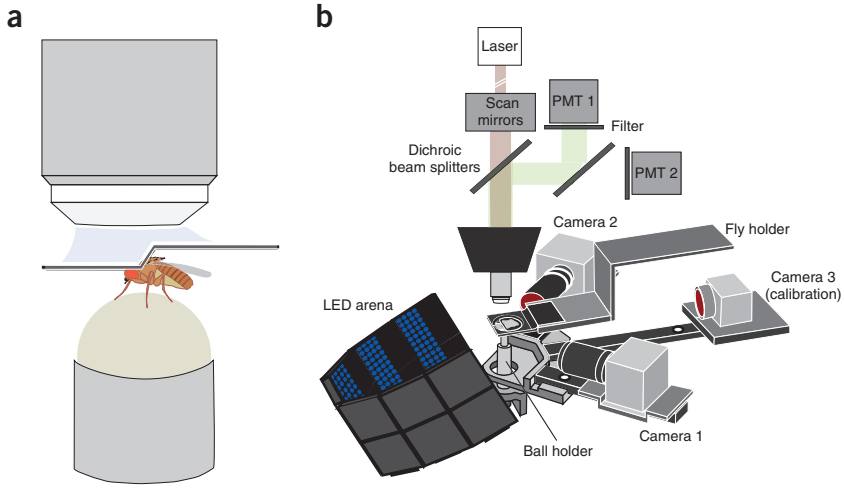

Figure 1 | Setup for two-photon imaging from the brain of head-fixed flies walking on a ball. (**a**) Schematic of the fly holder for tethered walking fly recording. Exposed fly brain is separated from intact legs and eyes allowing visual stimulation and walking on the ball. (**b**) Schematic showing arrangement of holder, ball, ball trackers, calibration camera, microscope (including a schematic for two-photon excitation and detection systems), objective and visual arena. PMT, photomultiplier tube.

We placed the fly chamber inside a larger setup that allows the fly to stand on a small air-supported ball (**Fig. 1b** and **Supplementary Fig. 2c,d**). We used two cameras to watch the fly and position it centrally on the ball with micromanipulators. As a visual aid we used still images from high-speed video recordings of flies walking freely in a 'ballscape' (**Supplementary Fig. 2e**). Behavioral experiments have been previously performed with *Drosophila* walking on an air-supported Styrofoam ball[30,31]. We used a custom-made polyurethane foam ball that had low inertia, a homogeneous distribution of mass, texture that allowed our sensors to detect small movements and a surface on which flies walked smoothly.

We tracked the ball's movements at high temporal resolution using a system based on a sensor chip that is commonly used to perform optical flow measurement in optical computer mouse devices. We integrated the sensor into a custom-designed circuit that streams ball velocity data to a computer at 4 kHz. Such a real-time readout makes the tracker suitable for future closed-loop experiments.

Optical computer mouse sensors have been used for larger insects[32], but the small size of our ball limits how close to it we can

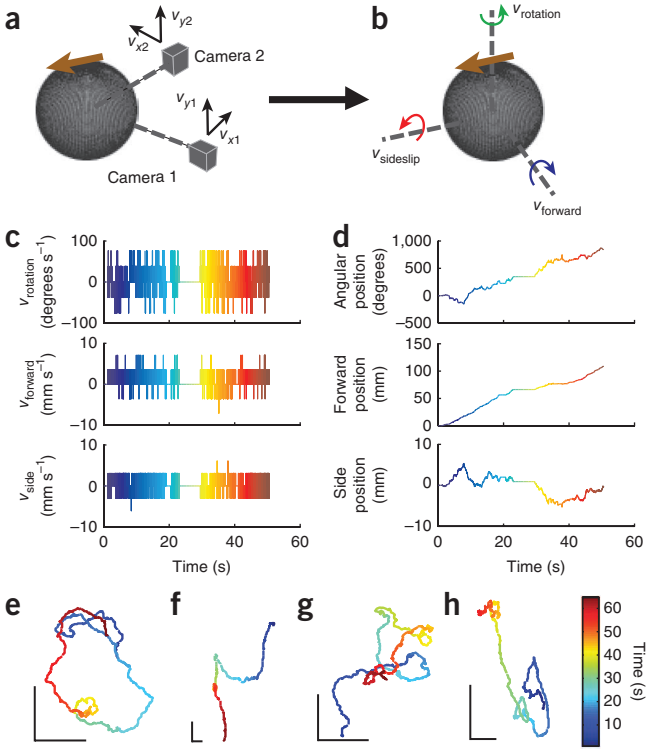

Figure 2 | High-precision ball tracking system allows online measurement of fly's virtual trajectory. (**a**) Cameras 1 and 2 capture *x* and *y* velocities (v_x and v_y) in their respective fields of view. Together, they provide 4-kHz tracking of the ball's rotation about all three axes. The brown arrow shows the fly's orientation on the ball. (**b**) The tethered fly's translational ($v_{forward}$ and $v_{sideslip}$ forward and sideslip velocity, respectively) and rotational ($v_{rotational}$) velocities on a virtual two-dimensional surface, obtained from rotational velocities of the ball. (**c**,**d**) Instantaneous velocity (5-ms bins) of a representative walking fly (**c**) and the accumulated displacement and rotation of the fly (**d**). (**e**–**h**) Fly displacement for four different flies walking without motion stimuli plotted as a virtual trajectory on a flat surface. Scale bars, 10 mm. Velocities for trajectory shown in **e** are shown in **c**. Progression of time in **c**–**h** is indicated by the color scale in **h**.

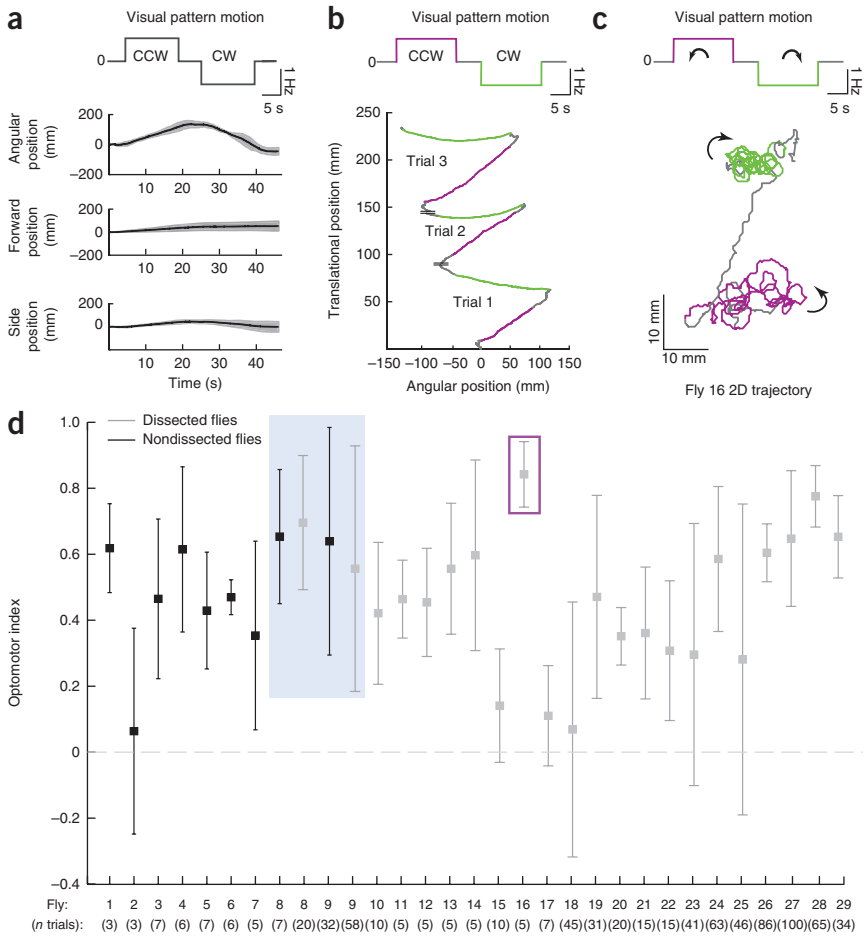

Figure 3 | Optomotor behavior in tethered flies. (**a**) Rotational and translational velocity of one fly (fly 16) in response to clockwise (CW) and counterclockwise (CCW) motion stimuli. The fly's rotational velocity, plotted as mean ± s.d. in gray ($n = 5$). (**b**,**c**) Translational and rotational movement (**b**) and virtual trajectory (**c**) of fly 16 in response to the motion stimulus. Schematics in **a**–**c** indicate motion-stimulus protocol and color codes used; 0 indicates no motion. (**d**) Summary plot of optomotor indices (mean ± s.d.; n values are indicated in the figure). Gray box highlights optomotor performance before and after dissection for two flies. Trials highlighted in magenta are those shown in **b**. Dashed line represents no optomotor response.

place the sensors. We thus used lenses to project the images of small regions of the ball close to the equator onto two sensors placed 90 degrees apart from each other and behind the fly. Each camera provided local x and y velocity information (**Fig. 2a**), but use of both cameras allowed us to track all velocity components of the ball. We could accurately transform local displacements of an approximately flat patch of the ball, as measured by the camera sensors, to a global rotation of the ball because the high rate of motion measurements ensures that only small displacements are captured. This allowed us to make implicit use of the small angle approximation.

We converted the ball velocities into rotational, forward and sideslip velocities for the fly (**Fig. 2b**–**d**). We then plotted trajectories that the fly would create if it were walking on flat ground (**Fig. 2e**–**h** and **Supplementary Movies 2** and **3**), with the limitation that the high local curvature of the ball we used made strict equivalence impossible. Subtle biases in positioning of the fly on the ball were manifested as biases in spontaneous walking in one direction or the other (**Fig. 2f**). We could partially correct for these biases by repositioning the fly, but for many tasks of interest, we used relative metrics (left versus right comparisons) that minimized these biases.

We used a modular LED arena to present visual stimuli to the fly[33]. To prevent light emitted by the display from reaching the photomultiplier tubes of the microscope, we used two sets of filters. We placed the first set of filters in front of the LED panels and placed a bandpass filter before the photomultiplier tubes. Remaining bleed-through contributed a constant background (**Supplementary Fig. 3**) that we subtracted from the fluorescence of the neuronal region of interest.

Optomotor behavior in the fly during physiology

Performing physiology experiments necessitates placing several constraints on the flies. In our experiment, we removed from flies some of their cuticle and exposed their brains. The flies' visual field was also somewhat reduced (Online Methods). The fly's ability to perform the behavior of interest under these conditions is a critical test of the usefulness of this preparation. We presented the fly with horizontally rotating vertical grating pattern moving at a temporal frequency (f_t) of 1 Hz, a stimulus that is known to evoke stereotypical compensatory turning responses in freely walking[34] and tethered walking flies[30]. We used two different motion-stimulus protocols to characterize the optomotor behavior in our rig. The protocols differed only in duration, with each featuring epochs of movement in the preferred and null directions of the recorded HS neuron. Trials lasted either 35 or 75 s depending on the protocol used, during which flies walked most of the time. Experiments lasted up to 4 h. For analysis, we rejected any trial in which the fly did not walk for more than 30% of the time (mean percentage of rejected trials = 14%, number of imaged flies = 19, number of trials ranged from 5 to 100; **Supplementary Fig. 4**).

We defined an optomotor response index (Online Methods) to quantify the optomotor response of the fly as the ratio between the difference of rotation velocities in preferred and null direction segments and the sum of the absolute value of rotation velocities in these segments. We ran several trials under dark and stationary stimulus conditions to test the motion-stimulus-dependence of the optomotor response index. (**Supplementary Fig. 5a**,**b**). We evaluated flies 1–17 using protocol 1 and flies 18–29 using protocol 2 (Online Methods). We found no difference in the behavior under the two different protocols (mean optomotor response index with protocol 1, 0.48 ± 0.20 and with protocol 2, 0.45 ± 0.21; $P = 0.6702$, Mann-Whitney). We also compared the walking and optomotor performance of flies on the ball to that of flies allowed to walk freely in a visual arena. Freely walking flies had consistently higher

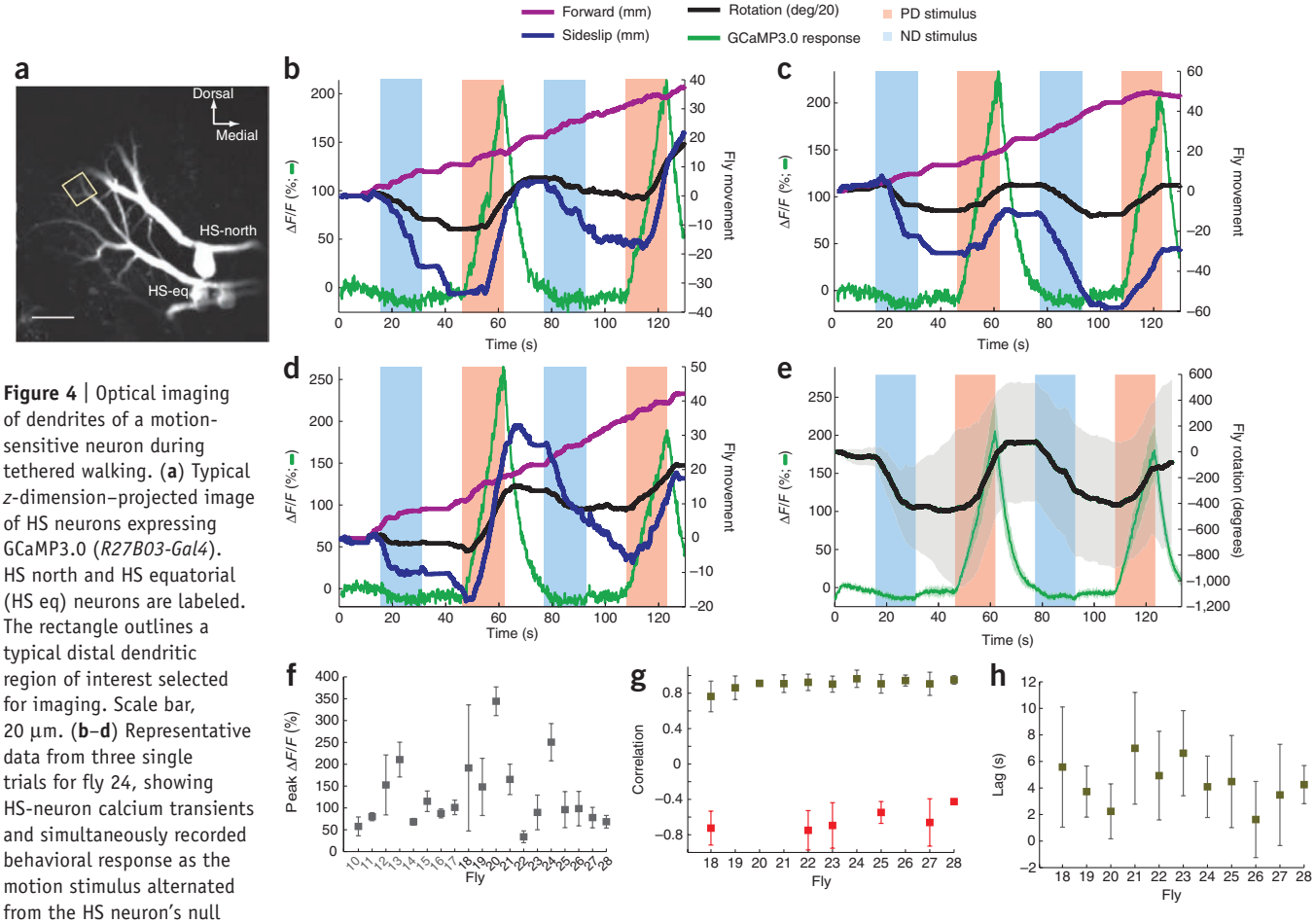

Figure 4 | Optical imaging of dendrites of a motion-sensitive neuron during tethered walking. (**a**) Typical *z*-dimension–projected image of HS neurons expressing GCaMP3.0 (*R27B03-Gal4*). HS north and HS equatorial (HS eq) neurons are labeled. The rectangle outlines a typical distal dendritic region of interest selected for imaging. Scale bar, 20 µm. (**b**–**d**) Representative data from three single trials for fly 24, showing HS-neuron calcium transients and simultaneously recorded behavioral response as the motion stimulus alternated from the HS neuron's null direction (ND) to preferred direction (PD). Note that rotation is shown in degs/20 for ease of plotting with forward and sideslip movement. Δ*F*/*F*, change in fluorescence intensity normalized by baseline fluorescence intensity. (**e**) Combined data (mean ± s.d. (gray shading)) from seven trials for fly 24 showing accumulated rotation and HS-neuron calcium transients during motion stimulation. (**f**) Mean ± s.d. (*n* values as in **Fig. 3d**) of difference between peaks of PD and ND calcium transients across trials for all flies imaged. (**g**) Peak correlations between calcium responses of HS neurons and rotational response to PD stimulation for flies subjected to protocol 2, and shown are data (mean ± s.d.) for trials with positive optomotor response index. Data (mean ± s.d) for occasional trials with negative correlations are shown in red (numbers of trials with positive and negative correlations for flies 18–28 were, respectively: 19/6, 12/0, 3/0, 8/0, 8/3, 27/4, 54/0, 17/2, 78/0, 81/14 and 63/1). (**h**) Lags between optomotor and calcium response across trials and flies measured from onset of calcium response to onset of behavioral rotational response for trials with positive correlation. All flies (except fly 20) displayed lags significantly greater than zero (*P* values for *t*-tests for lag distributions being significantly different from normal distribution around 0 for flies 18–28 were 6×10^{-5}, 7.5×10^{-3}, 0.27, 3.2×10^{-3}, 0.01, 4×10^{-10}, 6×10^{-17}, 3×10^{-4}, 4×10^{-6}, 7×10^{-13} and 2×10^{-27}, respectively).

forward velocities but lower rotational velocities (**Supplementary Fig. 6**), something that may be expected given that tethered flies walk on a curved surface. As body turns are the dominant observable feature of orientation behavior, the high rotational velocities of tethered flies walking on the ball suggest that our system is well suited for studying fly navigation.

Most flies showed behavioral responses during imaging, switching from turning in one direction to the other as the stimulus direction changed (**Fig. 3a–c** and **Supplementary Movies 2** and **3**). Dissected flies had optomotor responses that were comparable to those of nondissected flies, as measured by the optomotor response index (mean optomotor response index was 0.48 ± 0.19 for nondissected flies and 0.46 ± 0.21 for dissected flies; $P = 0.74$, Mann-Whitney; **Fig. 3d**). Moreover, in two flies we evaluated the optomotor behavior before and after dissection and found that their performance was not significantly different (fly 8, $P = 0.93$ and fly 9, $P = 0.41$; Mann-Whitney). Flies in our preparation could consistently turn in the direction of a motion stimulus, and the extent of their turning response in one direction versus the other was preserved in dissected, head-fixed configurations.

Two-photon imaging of HS neurons during optomotor behavior

To evaluate our preparation's suitability for imaging neuronal activity during walking behavior, we focused on HS neurons. There are three HS neurons in each *Drosophila* optic lobe[35], with receptive fields arranged along the dorsal-ventral axis (HS north, HS equator and HS south). Each neuron responds selectively to horizontal motion in its visual field and in its preferred direction, which is always the direction of expected optic flow for a forward-walking fly (called progressive or front-to-back motion). Different experimental strategies have shown the involvement of these neurons in the optomotor responses of *Calliphora*[36–38] and of *Drosophila*[39]. The HS neurons have also been the subject of imaging[40,41] and electrophysiological[26,27,42] studies in *Calliphora* and, recently, in *Drosophila*[23] as well, and their responses to motion stimuli have been thoroughly characterized.

We performed two-photon calcium imaging from HS neurons in *Drosophila*. We expressed the genetically encoded calcium indicator GCaMP3.0 (ref. 24) selectively in HS neurons using the *R27B03-Gal4* driver from the Rubin *Gal4* collection[43].

We presented the fly with vertical stripes rotating horizontally with f_t = 1 Hz and recorded HS-neuron calcium transients in the soma (**Supplementary Movie 4**) and dendrites (**Fig. 4a**,**b** and **Supplementary Movie 5**) along with the fly's behavioral responses. We looked at dendritic arbors because LPTC calcium transients are thought to be greater there than calcium transients in axonal arbors[41]. HS neurons responded to motion in their preferred direction with slow increases in fluorescence signals, in agreement with results using synthetic calcium indicators in the blowfly[40]. Calcium transients decayed slowly back to baseline levels after the preferred-direction stimulus was removed. We observed slight decreases in fluorescence signals during null-direction stimulation when recording from the soma, but these decreases were difficult to detect in the dendrites in which fluorescence intensities were lower (data not shown). The fly's turning response to motion stimuli in the preferred direction of the recorded HS neuron lagged behind the calcium responses. We recorded behavioral traces simultaneously with dendritic calcium transients (**Fig. 4b–e** and **Supplementary Movie 4**). Direct correlations between the preferred-direction phase of fluorescence signals with behavioral responses revealed a mean lag of 4.37 ± 1.65 s for the turning responses relative to dendritic calcium transients as measured by substantial deviations (>3 s.d.) from baseline (Online Methods). In all flies, we observed high correlations for most trials (**Fig. 4f–h**; variability in the data shown in **Fig. 4f** mainly reflects differences between imaging in different regions of interest). Our results were consistent with the involvement of HS neurons in the fly's optomotor response[25,36,37].

A key concern when monitoring HS-neuron responses during walking is the possibility that observed changes result from motion artifacts rather than neural activity. Although many different algorithms have been proposed for motion compensation, we found that translational compensation[44] sufficed in our experiments, which typically featured single, spatially localized regions of interest. If motion appeared to be out of plane or to have shear that made analysis difficult, we did not use the data. We verified our results using flies expressing cytosolic EGFP (**Supplementary Fig. 5c**). This allowed us to use activity-insensitive protein to monitor fluorescence changes resulting from any brain motion. We found that changes in fluorescence induced by brain motion artifacts could not explain the fluorescence transients observed during visual stimulation.

DISCUSSION

For spiking neurons in the fly, the correlation between spiking activity and genetically encoded calcium indicator signal can be problematic[10,45]. Thus, results obtained with these indicators need to be interpreted with some caution. The absence of a fluorescence signal does not necessarily imply absence of neural activity. In the blowfly, calcium dynamics of HS neurons have been well-characterized using synthetic indicators that accurately track calcium dynamics[41]. Such experiments suggest that voltage-dependent channels contribute to the observed signals. Calcium dynamics are likely to be similar in *Drosophila*, but this has not yet been shown. Despite such complexities, two-photon imaging with genetically encoded calcium indicators offer the vital advantage of cell specificity and high spatial resolution, providing a less invasive means of monitoring neural processing in arbors distant from the soma. Although electrophysiological techniques are irreplaceable for answering certain classes of questions, imaging provides the opportunity to monitor neuronal signals in different compartments of neurons and address questions related to single-cell signal processing. Additionally, long-term electrophysiological recordings are difficult to achieve in small neurons deep inside the brain, but two-photon imaging enables such recordings with high spatial resolution. Imaging also enables recording from populations of neurons and multiple dendritic arbors, which is likely to be important for understanding neural circuit function. Continuing improvements in the development of genetically encoded indicators suggest that imaging will be an increasingly powerful approach for investigating neural circuit dynamics in *Drosophila* in the future.

Flies display various behaviors while walking, many of which are understudied. Our setup allows high-temporal-resolution monitoring of fly neural activity and movements, with flies demonstrating robust optomotor behavior for several hours. The strong optomotor performance we observed in flies on the rig suggests that we should also be able to reproduce more complex behaviors under the two-photon microscope. For example, both open- and closed-loop physiological experiments, with *Drosophila* performing adaptive behaviors in a precisely controlled sensory environment, now appear feasible. Ever-expanding tools allow expression of genetically encoded sensors, activators and repressors of neural activity in subsets of neurons in the entire fly brain, and these targeted manipulations can be reliably reproduced for different flies. The combination of such tools with targeted physiological recordings in behaving flies during both walking and flying[15] (J.D.S., M.B.R. and V.J.; unpublished data) should enable systematic, multiscale investigations into questions about sensorimotor processing and learning and memory that are at present difficult to address mechanistically in other organisms.

METHODS

Methods and any associated references are available in the online version of the paper at http://www.nature.com/naturemethods/.

Note: Supplementary information is available on the Nature Methods website.

ACKNOWLEDGMENTS

We thank J. Simpson and S. Hampel for cloning GCaMPs into pMUH; D. Hall and K. Hibbard for fly crossing; members of Janelia's Fly Core and particularly G. Zhang for stock maintenance; K. Svoboda for donations of equipment and for advice in setting up our two-photon microscopes; D. Flickinger, S. Bassin, T. Tabachnik and C. Werner for contributions to the optical and mechanical design; V. Iyer for developing new ScanImage features and for support; T. Ofstad for assistance with free-walking experiments; N. Kladt for assistance with calibration experiments; M. Ahrens for software contributions and P. Coen for carrying out pilot experiments with the ball tracker. B. Pfeiffer and G. Rubin (Janelia Farm) provided pMUH. G. Rubin gifted us *R27B03-Gal4*. For pilot experiments, D. Reiff (Max Planck Institute, Martinsried) provided *DB331-Gal4* and L. Luo (Stanford University) provided line *3A-Gal4*. We received generous advice and support from others at Janelia Farm, including members of the Svoboda lab. This work was supported by the Howard Hughes Medical Institute.

AUTHOR CONTRIBUTIONS

J.D.S., M.E.C., G.K.L., M.B.R. and V.J. designed the project. J.D.S. designed the fly-physiology-with-behavior preparation with input from J.E.O., M.E.C. and V.J.; J.D.S., M.E.C., A.D., J.E.O. and V.J. designed the mechanical setup; M.B.R., J.D.S.

and M.E.C. designed the LED arena; G.K.L. designed the ball tracker with input from M.B.R. and V.J.; M.E.C., J.D.S., M.B.R. and V.J. calibrated the tracker; V.J. performed high-speed video experiments; J.D.S. performed free-walking behavior experiments; J.D.S. and M.E.C. performed all other behavior and physiology experiments; J.D.S., M.E.C. and V.J. performed data analysis; M.E.C. performed fly crosses; and V.J., J.D.S., M.E.C., G.K.L. and M.B.R. wrote the paper.

COMPETING FINANCIAL INTERESTS

The authors declare no competing financial interests.

Published online at http://www.nature.com/naturemethods/.
Reprints and permissions information is available online at http://npg.nature.com/reprintsandpermissions/.

1. Vosshall, L.B. Into the mind of a fly. *Nature* **450**, 193–197 (2007).
2. Olsen, S.R. & Wilson, R.I. Cracking neural circuits in a tiny brain: new approaches for understanding the neural circuitry of *Drosophila*. *Trends Neurosci.* **31**, 512–520 (2008).
3. Borst, A. *Drosophila*'s view on insect vision. *Curr. Biol.* **19**, R36–R47 (2009).
4. Simpson, J.H. Mapping and manipulating neural circuits in the fly brain. *Adv. Genet.* **65**, 79–143 (2009).
5. Gouwens, N.W. & Wilson, R.I. Signal propagation in *Drosophila* central neurons. *J. Neurosci.* **29**, 6239–6249 (2009).
6. Peron, S.P., Krapp, H.G. & Gabbiani, F. Influence of electrotonic structure and synaptic mapping on the receptive field properties of a collision-detecting neuron. *J. Neurophysiol.* **97**, 159–177 (2007).
7. Haag, J. & Borst, A. Neural mechanism underlying complex receptive field properties of motion-sensitive interneurons. *Nat. Neurosci.* **7**, 628–634 (2004).
8. Denk, W., Strickler, J.H. & Webb, W.W. Two-photon laser scanning fluorescence microscopy. *Science* **248**, 73–76 (1990).
9. Wang, J.W., Wong, A.M., Flores, J., Vosshall, L.B. & Axel, R. Two-photon calcium imaging reveals an odor-evoked map of activity in the fly brain. *Cell* **112**, 271–282 (2003).
10. Jayaraman, V. & Laurent, G. Evaluating a genetically encoded optical sensor of neural activity using electrophysiology in intact adult fruit flies. *Front. Neural Circuits* **1**, 3 (2007).
11. Ng, M. *et al.* Transmission of olfactory information between three populations of neurons in the antennal lobe of the fly. *Neuron* **36**, 463–474 (2002).
12. Churchland, M.M., Afshar, A. & Shenoy, K.V. A central source of movement variability. *Neuron* **52**, 1085–1096 (2006).
13. Bohm, H., Schildberger, K. & Huber, F. Visual and acoustic course control in the cricket Gryllus-Bimaculatus. *J. Exp. Biol.* **159**, 235–248 (1991).
14. Mason, A.C., Oshinsky, M.L. & Hoy, R.R. Hyperacute directional hearing in a microscale auditory system. *Nature* **410**, 686–690 (2001).
15. Maimon, G., Straw, A.D. & Dickinson, M.H. Active flight increases the gain of visual motion processing in *Drosophila*. *Nat. Neurosci.* **13**, 393–399 (2010).
16. Evarts, E.V. Relation of pyramidal tract activity to force exerted during voluntary movement. *J. Neurophysiol.* **31**, 14–27 (1968).
17. Wurtz, R.H. Visual cortex neurons: response to stimuli during rapid eye movements. *Science* **162**, 1148–1150 (1968).
18. Ono, T., Nakamura, K., Nishijo, H. & Fukuda, M. Hypothalamic neuron involvement in integration of reward, aversion, and cue signals. *J. Neurophysiol.* **56**, 63–79 (1986).
19. Dombeck, D.A., Khabbaz, A.N., Collman, F., Adelman, T.L. & Tank, D.W. Imaging large-scale neural activity with cellular resolution in awake, mobile mice. *Neuron* **56**, 43–57 (2007).
20. Egelhaaf, M. *et al.* Neural encoding of behaviourally relevant visual-motion information in the fly. *Trends Neurosci.* **25**, 96–102 (2002).
21. Borst, A. & Haag, J. Neural networks in the cockpit of the fly. *J. Comp. Physiol. A Neuroethol. Sens. Neural Behav. Physiol.* **188**, 419–437 (2002).
22. Joesch, M., Plett, J., Borst, A. & Reiff, D.F. Response properties of motion-sensitive visual interneurons in the lobula plate of *Drosophila melanogaster*. *Curr. Biol.* **18**, 368–374 (2008).
23. Schnell, B. *et al.* Processing of horizontal optic flow in three visual interneurons of the *Drosophila* brain. *J Neurophysiol.* **103**, 1646–1657 (2010).
24. Tian, L. *et al.* Imaging neural activity in worms, flies and mice with improved GCaMP calcium indicators. *Nat. Methods* **6**, 875–881 (2009).
25. Hausen, K. & Wehrhahn, C. Neural circuits mediating visual flight control in flies. I. Quantitative comparison of neural and behavioral response characteristics. *J. Neurosci.* **9**, 3828–3836 (1989).
26. Hausen, K. Motion sensitive interneurons in the optomotor system of the fly. 1. The horizontal cells—structure and signals. *Biol. Cybern.* **45**, 143–156 (1982).
27. Hausen, K. Motion sensitive interneurons in the optomotor system of the fly. 2. The horizontal cells—receptive-field organization and response characteristics. *Biol. Cybern.* **46**, 67–79 (1982).
28. Lehmann, F.O. & Dickinson, M.H. The changes in power requirements and muscle efficiency during elevated force production in the fruit fly *Drosophila melanogaster*. *J. Exp. Biol.* **200**, 1133–1143 (1997).
29. Strausfeld, N.J. The head-neck system of the blowfly *Calliphora*. in *The Head-Neck Sensory Motor System*. (eds., Berthoz, A., Graf, W. and Vidal, P.P.) 56–63 (Oxford University Press, 1992).
30. Gotz, K.G. & Wenking, H. Visual control of locomotion in the walking fruitfly. *Drosophila*. *J. Comp. Physiol. A Neuroethol. Sens. Neural Behav. Physiol.* **85**, 235–266 (1973).
31. Buchner, E. Elementary movement detectors in an insect visual-system. *Biol. Cybern.* **24**, 85–101 (1976).
32. Lott, G.K., Rosen, M.J. & Hoy, R.R. An inexpensive sub-millisecond system for walking measurements of small animals based on optical computer mouse technology. *J. Neurosci. Methods* **161**, 55–61 (2007).
33. Reiser, M.B. & Dickinson, M.H. A modular display system for insect behavioral neuroscience. *J. Neurosci. Methods* **167**, 127–139 (2008).
34. Strauss, R., Schuster, S. & Gotz, K.G. Processing of artificial visual feedback in the walking fruit fly *Drosophila melanogaster*. *J. Exp. Biol.* **200**, 1281–1296 (1997).
35. Scott, E.K., Raabe, T. & Luo, L. Structure of the vertical and horizontal system neurons of the lobula plate in *Drosophila*. *J. Comp. Neurol.* **454**, 470–481 (2002).
36. Hausen, K. & Wehrhahn, C. Microsurgical lesion of horizontal cells changes optomotor yaw responses in the blowfly *Calliphora Erythrocephala*. *Proc. Biol. Sci.* **219**, 211–216 (1983).
37. Geiger, G. & Nassel, D.R. Visual orientation behaviour of flies after selective laser beam ablation of interneurones. *Nature* **293**, 398–399 (1981).
38. Blondeau, J. Electrically evoked course control in the fly Calliphora Erythrocephala. *J. Exp. Biol.* **92**, 143–153 (1981).
39. Heisenberg, M., Wonneberger, R. & Wolf, R. Optomotor-blind—*Drosophila* mutant of lobula plate giant neurons. *J. Comp. Physiol.* **124**, 287–296 (1978).
40. Durr, V. & Egelhaaf, M. In vivo calcium accumulation in presynaptic and postsynaptic dendrites of visual interneurons. *J. Neurophysiol.* **82**, 3327–3338 (1999).
41. Haag, J. & Borst, A. Spatial distribution and characteristics of voltage-gated calcium signals within visual interneurons. *J. Neurophysiol.* **83**, 1039–1051 (2000).
42. Haag, J. & Borst, A. Active membrane properties and signal encoding in graded potential neurons. *J. Neurosci.* **18**, 7972–7986 (1998).
43. Pfeiffer, B.D. *et al.* Tools for neuroanatomy and neurogenetics in *Drosophila*. *Proc. Natl. Acad. Sci. USA* **105**, 9715–9720 (2008).
44. Guizar-Sicairos, M., Thurman, S.T. & Fienup, J.R. Efficient subpixel image registration algorithms. *Opt. Lett.* **33**, 156–158 (2008).
45. Reiff, D.F. *et al. In vivo* performance of genetically encoded indicators of neural activity in flies. *J. Neurosci.* **25**, 4766–4778 (2005).

ONLINE METHODS

Fly stocks. Flies were reared on standard cornmeal agar under a 12-h light and 12-h dark cycle at 25 °C. All experiments were performed on adult female flies, 2–4 d after eclosion. Stocks were generously provided as follows: *R27B03-Gal4* (G. Rubin and A. Nern), *UAS-GCaMP3.0* (L. Looger and J. Simpson). Line R27B03 was constructed as previously described[43] and identified as driving expression in the HS neurons (A. Nern; unpublished data).

Fly holder. The details of the holder geometry are shown in **Supplementary Figs. 1** and **2a**. The lower side of the fly holder is painted black using a metal staining opaque paint (Dykem opaque staining; ITW Dymon) to avoid reflections of the visual stimulus on the shim surface that could affect fly behavioral responses. This holder is robust and reusable.

Fly preparation and positioning on the ball. A female fly was anesthetized on ice and transferred to a cold plate. We fixed the extended proboscis of the fly with a wax mixture (1:1 molten bee wax and colophony, Sigma Aldrich) to minimize motion of the brain.

Under a dissection microscope we glued a pin to the anterior third of the fly's thorax at a 45–60° angle and inserted the pin into a mount attached to a three-axis micromanipulator to position the fly's head and thorax in the holder. This was done above a cold stage to minimize fly movement. The head of the fly was bent forward by about 70–80° to give access to its posterior surface and glued to the holder with UV light–activated glue (Fotoplast gel; Dreve). The glue was spread along the head using a pulled glass capillary with a small glass ball of about 40 µm diameter at its end. The glue was cured after each step using UV light (LED-100 UV portable; Electro-lite Corp) for about 20 s. After gluing the head, the fly was lowered slightly using the micromanipulator and moved backwards to relax neck tension and give good optical access to the dorsal part of the head and the LPTCs (**Supplementary Fig. 2b**). Any uncured glue at the surface was removed using a paper tissue and extensive rinsing with saline.

Under saline solution[46] with 2 mM Ca^{2+}, we used sharpened #5 forceps to carefully remove the cuticle and some of the fat tissue preventing optical access to the LPTCs (**Supplementary Fig. 2b**). Calcium signals can easily be lost if the neural processes are damaged during the dissection. We also removed the muscle M16 (ref. 10) to prevent brain motion. The procedure lasted about 40 min. Most flies that were fixed in the holder did not immediately show walking behavior after being positioned on the ball. Consistent walking behavior (for example, **Supplementary Movie 1**) developed soon after the fly adapted to the ball. The adaptation was mostly due to the positioning of the fly in the holder. If flies adapted to the ball, they quickly began walking behavior after the dissection and could maintain it for up to 4 h (for example, **Supplementary Fig. 7**).

Treadmill ball. Previous *Drosophila* walking experiments on an air-supported ball have used a Styrofoam ball with a diameter of 7–9 mm and a weight of 10 mg[31,47]. When testing a Styrofoam ball with these specifications, we noticed that flies easily lifted the ball. We used a ball of 40 mg (6-mm diameter) manufactured from polyurethane foam (Last-A-Foam; General Plastics Manufacturing Company) using a bowl shaped file with an inner diameter of 6 mm (**Supplementary Fig. 8a**). The edge of the file is sharp and the radial surface is textured using electrical-discharge machining. This results in a surface texture similar to a nail file. With the ball file inserted into a hand-held drill, a piece of polyurethane foam was slowly rotated against the ball file until it became a sphere with a diameter of 6 mm. The ball can be coated with polyurethane spray paint to prevent small dust particles from coming off the ball.

Ball holder and flow meter. The ball floats on a stream of air[31]. The ball holder had a hemispherical bowl for the ball (**Supplementary Fig. 8b**). The bowl was lightly smoothed using a glass bead abrasion machine. The airflow was adjusted using a flow-meter (correlated flowmeter, maximum flow rate: 825 ml min^{-1}; Cole-Parmer).

High-resolution ball tracker. To track the movement of the air-supported ball, we developed a custom high-speed 'optical flow camera' based on a commercially available motion-sensing chip (Avago Technologies; ADNS-6090). The ADNS-6090 measures optical flow based on sequential correlations of 30 × 30–pixel images, with a maximum frame rate of 7.2 kHz. The ADNS-6090 can acquire snapshot video frames of its visual field and stream the pixel data at video rates (20 Hz). Our camera system consisted of three discrete units: two cubical camera enclosures with c-mount lens threads and a single microcontroller unit (MCU) base unit to which the cameras were connected via ten wire-ribbon cables (**Supplementary Fig. 9**).

Tracker: microcontroller core, signal conditioning, signal input and output, and power. The interface between the ADNS-6090 and the PC was mediated by a deterministic microcontroller with a 20 MHz quartz oscillator. The controller responds to commands from the PC user, acquires data at a fixed sample rate and conditions data for return to the PC or to the real-time interface.

The Atmel ATMega644p is at the core of our system. Firmware was developed for the Atmel microcontroller in the CodeVisionAVR C development environment and programmed to the device via a universal serial bus (USB) in-system programmer (Atmel AVR ISP mkII).

The MCU was driven at 5 V, provided by the USB data cable, for transistor-transistor logic (TTL) level compatibility through the real-time interface. Conversion to 3.3 V logic for communication with the ADNS sensor chip was accomplished with noninverting precision Schmitt-triggers. The MCU communicated with the ADNS-6090 via a six-line serial interface. This interface operated at 3.3 V and was clocked in a custom serial 'bit-banging' fashion to send identical data to both chips while reading responses from the cameras on separate parallel lines. The bit stream can be paused and continued during operation.

Serial port communication with a PC was accomplished via a universal asynchronous receiver/transmitter (UART) to USB converter (FTDI FT232BL). In our implementation, the serial interface operated with a data rate of 1 Mbit s^{-1}. An analog representation of the motion signals (accumulated over a user-selectable fixed time interval) was generated on four external lines for each of the four principal axis velocities during operation. Four channels of analog output were provided by a 12-bit parallel 4-channel digital to analog converter. This parallel addressed

device allowed for simultaneous latching of output values to prevent sample phase lag across output channels.

Tracker: firmware state machine and data packet format. The majority of the firmware code for the MCU consists of a user interface state machine that responds to multiple byte commands from the PC user. Fixed byte commands control the state of the system in either 'idle', 'video streaming' or 'motion data streaming' modes. Other commands allow for a communications bridge between the PC user and the internal configuration and status registers of the ADNS-6090.

Data streaming to a PC is timed by a dedicated interrupt service routine driven by the system quartz oscillator signal. During the data read from the cameras, the MCU services UART transmit interrupts so as to deliver data to the PC user while concurrently acquiring new data from the ADNS-6090 chips in an interleaved fashion.

The serial data stream consists of packets containing a header byte, a counter byte that loops over the 0–255 range and a programmable number of bytes including *x*-*y* velocity values from each camera or combined pitch/roll/yaw/blank values (4 bytes), camera surface quality values (2 bytes) and 16-bit shutter speed values (4 bytes). The overall system sample rate is primarily limited by the time to read values from the ADNS camera chips and may be increased by reducing the data packet size.

Tracker: camera housing, mounting frame, lenses and illumination. The ADNS sensor was delivered with a bushing that is designed to direct light onto the chip from an integrated illumination source at a prescribed angle to the package in typical optical mouse applications. The bushing may be removed by releasing a set of plastic tabs at either end of the long axis of the package.

The plastic frame of the chip is soldered in place so as to be flush against the back surface of a circuit board mounted inside a custom-anodized aluminum frame (**Supplementary Fig. 10**). We visualized the moving surface through a 25 mm closed-circuit television lens, a 2× lens extender and a 1-inch extension tube.

Tracker: calibration and optical alignment of the tracking system. To align the tracking cameras, we used a cubical target that fit into the air support stand. We calibrated the tracking system and tested the linearity of the motion measurement by directly controlling the rotational velocity of the ball. The ball was attached to a servo motor (Compumotor SM161AE-NGSN, controlled by a Gemini GV Servo Drive; Parker Motion Control Systems), which rotated at constant velocities for different durations. We derived a velocity calibration factor by comparing the velocities measured with the tracking system to known (command) ball velocities (**Supplementary Fig. 11a**). The calibration was well fit by a linear regression, with a coefficient of regression of 0.99 (clockwise rotations, $n = 10$; counterclockwise rotations, $n = 10$). Moreover, the calibration factor was constant across all tested velocities. We examined the precision of the system by testing its performance during movement onsets and stops. The tracker responded reliably across all velocities tested with a tick for every 80 μm at the magnification used (**Supplementary Fig. 11b**). Simultaneous movement tracking with two cameras gave identical results in all trials (median difference across different displacements = 0, range form −1 to 1 arbitrary units, $n = 40$; **Supplementary Fig. 11c**).

Tracking performance depends on shutter speed and surface quality, which in turn depend on illumination conditions. We used 850-nm collimated infrared LEDs with flexible arms (SLFA-850-12-2-SA-110; Illumination Control, Inc.) illuminating the ball from a distance of 1–2 cm roughly parallel to the optical axis of the tracking cameras without obstructing the field of view to achieve the highest surface quality and shutter speeds (**Supplementary Fig. 12**). We ensured the consistency of tracking conditions by recording the ball's movement at a frame rate of 480 Hz at the beginning of each experiment using a third camera (**Fig. 1b**). This camera was placed directly behind the fly and had a similar field of view as the tracking cameras, with a resolution set to 100 × 100 pixels. We compared the ball's trajectory as determined by the tracking system to that obtained by the extra camera using offline Matlab (The MathWorks, Inc.) image processing code based on subimage cross-correlations. Briefly, two-axis movement of the ball was extracted from the recorded movie by subdividing the field of view into 100 subfields. The movement in the 36 center fields was computed by cross-correlation of the fields between subsequent frames using built-in Matlab functions (details and software are available at http://www.flyfizz.org/). We found a linear relationship between calibration factors computed from ball tracker output and camera-measured translation ($R^2 = 0.99 \pm 0.004$; **Supplementary Fig. 11d**). Given the close agreement between *x* and *y* calibration factors (6.6 ± 0.6 and 6.1 ± 0.6, respectively), we used the average of the two for the rotational calibration factor.

Tracker: reconstruction of the fly's walking trajectories. We used two tracking cameras (**Fig. 2a**) to acquire the ball's three rotational degrees of freedom, roll, pitch and yaw. The cameras were positioned at the equator of the ball at a distance of 8 to 10 cm and at 135° and −135° in the azimuth, with 0° degrees corresponding to the fly's body axis (in the ideal alignment condition; **Fig. 2a**,**b**). Both cameras tracked motion of the ball using their local view, measuring movement in the *x* (X_1 and X_2) and *y* (Y_1 and Y_2,) directions. We then extracted yaw (pure rotation of the fly, referred to as rotational velocity or velocity_rotation), pitch (velocity_forward) and roll (velocity_side) velocities as follows:

$$\text{velocity\_forward}_{\text{ball}} = (Y_1 + Y_2) \times \cos(\gamma), \text{with } \gamma = 45^{\circ}$$

and

$$\text{velocity\_side}_{\text{ball}} = (Y_1 - Y_2) \times \sin(\gamma),$$

$$\text{velocity\_rotation}_{\text{ball}} = (X_1 + X_2)/2.$$

Ball movement compensated for the fly's walking motion, and ball velocities therefore translated directly to virtual velocities of the fly. Thus,

$$\text{velocity\_forward}_{\text{fly}} = -\text{velocity\_forward}_{\text{ball}}$$

$$\text{velocity\_side}_{\text{fly}} = -\text{velocity\_side}_{\text{ball}}$$

$$\text{velocity\_rotation}_{\text{fly}} = -\text{velocity\_rotation}_{\text{ball}}.$$

We defined translational velocities as the square root of the sum of the squares of forward and side velocities. To reconstruct the fly's virtual two-dimensional trajectory we used both position and gaze. Briefly, for a coordinate system centered on the fly with a

doi:10.1038/nmeth.1468

y axis along the fly's body axis at its first position (0, 0, 0), if the fly's current coordinates on a virtual flat plane are (fly_x, fly_y, θ), its new position is

$$\theta_{\text{new}} = \theta + \text{velocity\_rotation}_{\text{fly}} \times \Delta t$$
$$\text{fly}_{x\text{new}} = \text{fly}_x + \text{velocity\_side}_{\text{fly}} \times \cos(\theta_{\text{new}}) - \text{velocity\_forward}_{\text{fly}} \times \sin(\theta_{\text{new}})$$
$$\text{fly}_{y\text{new}} = \text{fly}_y + \text{velocity\_side}_{\text{fly}} \times \sin(\theta_{\text{new}}) + \text{velocity\_forward}_{\text{fly}} \times \cos(\theta_{\text{new}}).$$

Tracker: Matlab software user interface. The Matlab-based interface software provides two functions: (i) control and calibration and (ii) data streaming and logging. One component is a visualization tool that streams the visual fields of the cameras ($2 \times 30 \times 30 = 1{,}800$ pixels) at a 20 Hz frame rate. The tracker data are either displayed in a two-dimensional field as independent points or applied as rotational transformations to a three-dimensional ball. The data path to and from the PC is mediated either via a virtual serial COM port or direct access to the Future Technology Devices International (FTDI) D2xx C based driver library.

Visual display arena and shielding. We used a modular LED arena to present visual stimuli to the fly[33]. The light of the blue LED arena (Bright LED Electronics Corp.; emission maximum at 465 nm) had to be filtered to avoid interference with fluorescence detection during two-photon imaging. The arena was covered with four layers of color filters (Kodak Wratten 47B). However, filtering was not complete and the remaining fluorescent background due to bleed-through-induced intensity, which peaked at 450 nm (full-width half-maximum = 45 nm), was typically 4 ± 2.8% $\Delta F/F$ (with respect to baseline fluorescence during arena–off conditions) for a photomultiplier tube gain of 0.405 V. This offset was (**Supplementary Fig. 3**) subtracted for each trial (see below). Moreover, in our calcium signal analysis, we defined the baseline during the segment of a stationary (not moving) pattern (see below). The maximal luminance of the visual arena with the filter was 0.85 cd m^{-2}.

The semicylinder arena was constructed from 14 modular LED panel displays with a resolution of 16 × 56 pixels, a height of 70 mm and a diameter of 123 mm. When the fly is positioned at the center, those dimensions span ~157° in azimuth and 45° in elevation with a maximum pixel subtense of 2.8°, all with respect to the fly's visual field. However, because the fly was on the ball, the subtended angle of elevation was reduced to ~40°. Horizontal moving patterns were generated with vertical bars of constant spatial period (wavelength = 22.4°) moving at 22.4° per second so that the temporal frequency (the angular velocity of the pattern divided by the spatial period) was 1 Hz. Patterns were generated in which three consecutive frames with intermediate intensity levels at the edges of the bars were used to define one pixel displacement. Large-field vertical gratings of maximal contrast were presented to the fly in two protocols, which differed only in trial length. Protocol 1 consisted of a 5-s stationary pattern segment after which the pattern moved horizontally in the preferred direction (PD) of the neuron for 10 s. After PD stimulation, another 5-s stationary pattern segment preceded motion of the pattern in the anti-preferred or null direction (ND) of the neuron for 10 s. The trial ended with 5 s of the stationary pattern. In protocol 2 both the stationary and moving segments lasted 15 s. Thus, trials run with protocol 1 lasted 35 s, whereas trials run with protocol 2 lasted 75 s.

Free walking behavior. Flies walked on a flat, round platform with a diameter of 95 mm surrounded by a cylindrical arena (360° in azimuth) that was constructed from panels identical to those used for tethered walking. However, the LED light was not filtered, which resulted in a slight green shift of the stimulus light and many times greater stimulus intensity. The walking platform was actively maintained at the same temperature as was used for the tethered experiments (21 °C). The flies were enclosed by a heated metal ring with a height of 3.8 mm that supported a glass plate coated with Sigmacote (Sigma-Aldrich; arena design, T. Ofstad and M.B.R.; unpublished data). We placed three 2–4-day-old flies at a time on the platform, and presented stationary, clockwise and counterclockwise stimulation with the same pattern used in the tethered walking experiments. Each stimulus condition lasted 15 s and the stimulus sequence was repeated for 20 min. We tracked the positions of walking flies at 15 frames per second with a camera (Basler 602f) from above. We obtained walking trajectories for each fly using Ctrax software[48] and calculated the translational and rotational velocities based on the distance moved between subsequent frames (75 ms). For averaging, we excluded parts where the fly was stationary (<1 mm s^{-1} translational velocity). Velocities of tethered flies were calculated as the change in position during 75 ms and were smoothed using Savitzky-Golay filtering with a span of 150 ms.

Two-photon imaging. We imaged on a custom-built two-photon microscope using ScanImage 3.6 software[49] and Olympus water immersion objectives (LUMPlanFl/IR, 60×, numerical aperture (NA), 0.9 and LUMPlanFl/IR, 40×, NA, 0.8). A mode-locked Ti:sapphire Chameleon Ultra II laser (Coherent) tuned to 920–930 nm was used as the excitation source. Fluorescence was collected using photomultiplier tubes (Hamamatsu) after bandpass filtering using a BG22 emission filter (Chroma Technologies) and either an HQ615/70-2p filter (Chroma Technologies) or FF01-680/SP-25 filter (Semrock). An additional filter was used to minimize bleed through of arena light (FF01-542/50-25; Semrock). Images were acquired in framescan mode (4–16 Hz). We noticed that using laser intensity much beyond 20 mW (measured at the back aperture) produced behavioral responses in flies (presumably due to heating[50]) and subsequently restricted the laser intensity to below 15 mW.

We only imaged the left half of the fly brain. Therefore, all HS neuron data shown were collected from the left HS neuron, for which PD corresponds to rotations in the counterclockwise direction.

Data analysis: two-photon imaging. Image processing was performed using custom code written and run in Matlab.

To correct motion artifacts during behavior, we implemented image registration of the raw image sequence by translational-compensation-based discrete Fourier analysis (efficient subpixel registration[44]). In most cases, we needed only minimal motion correction (**Supplementary Fig. 13**). Regions of interest were selected manually. Peak responses were calculated as the difference

between the mean of last second within the PD segment and the mean of the last second within the ND segment.

Data analysis: optomotor behavior. We defined an optomotor response index to quantify the optomotor response of the fly as follows (abs, absolute value):

$$\text{Optomotor index} = \frac{\sum V_{\text{CCW}} - \sum V_{\text{CW}}}{\sum \text{abs}(V_{\text{CCW}}) + \sum \text{abs}(V_{\text{CW}})},$$

with V_{CW} representing rotational velocity signals obtained when the pattern moved clockwise. Similarly V_{CCW} represents rotational velocity signals when the pattern moved counterclockwise. When the fly 'rotates' counterclockwise (that is, when the ball rotates clockwise), the fly's rotational velocity signals are positive. Conversely, when the fly 'rotates' clockwise (that is, the ball rotates counterclockwise), the rotational velocity signals are negative. The index ranges from 1 (pure optomotor response) to −1 (pure counteroptomotor response).

Data analysis: correlations between neuronal and behavioral responses. After selecting trials in which flies showed positive optomotor response index, cross-correlations were computed between behavioral responses (rotations) and fluorescence transients during PD stimulation. If zero-lag correlations were found to be negative, as was only rarely the case, we showed cross-covariance minima in **Figure 4g**. Otherwise, we took the positive peak of cross-covariances. For computing lags, only trials showing positive cross-covariances were used. Lags were computed across trials and flies as the delay between the measured onset of fluorescence response (3 s.d. greater than baseline) and the onset of behavioral response (angular rotation 3 s.d. greater than baseline in the direction of motion stimulus). For behavioral responses, we numerically corrected any baseline bias (caused by the fly favoring rotation toward one side over another before a stimulus is presented owing to minor imbalances in positioning). We first calculated a bias slope over the entire baseline period across trials and then used it to compute linear corrections for the entire trace.

46. Olsen, S.R., Bhandawat, V. & Wilson, R.I. Excitatory interactions between olfactory processing channels in the *Drosophila* antennal lobe. *Neuron* **54**, 89–103 (2007).
47. Bausenwein, B., Muller, N.R. & Heisenberg, M. Behavior-dependent activity labeling in the central complex, of *Drosophila* during controlled visual-stimulation. *J. Comp. Neurol.* **340**, 255–268 (1994).
48. Branson, K., Robie, A.A., Bender, J., Perona, P. & Dickinson, M.H. High-throughput ethomics in large groups of *Drosophila*. *Nat. Methods* **6**, 451–457 (2009).
49. Pologruto, T.A., Sabatini, B.L. & Svoboda, K. ScanImage: flexible software for operating laser scanning microscopes. *Biomed. Eng. Online* **2**, 13 (2003).
50. Hopt, A. & Neher, E. Highly nonlinear photodamage in two-photon fluorescence microscopy. *Biophys. J.* **80**, 2029–2036 (2001).

doi:10.1038/nmeth.1468

Corrigendum: Two-photon calcium imaging from head-fixed *Drosophila* during optomotor walking behavior

Johannes D Seelig, M Eugenia Chiappe, Gus K Lott, Anirban Dutta, Jason E Osborne, Michael B Reiser & Vivek Jayaraman
***Nat. Methods* 7, 535–540 (2010); published online 6 June 2010; corrected after print 10 January 2011.**

In the version of this article initially published, the units for angular position (degrees) in Figure 3a,b are incorrect. The correct unit should be mm. The error has been corrected in the HTML and PDF versions of the article.